PRAMANA
— journal of
physics

Vol. 84, No. 6
June 2015
pp. 987–997

Site-specific doping, tunable dielectric properties and intrinsic paramagnetism in Mn-doped $SrTiO_3$

D CHOUDHURY
Department of Physics, Indian Institute of Technology, Kharagpur 721 302, India
E-mail: debraj@phy.iitkgp.ernet.in

DOI: 10.1007/s12043-015-1002-z; ***e*Publication:** 29 May 2015

Abstract. Mn doping in $SrTiO_3$ leads to the emergence of qualitatively distinct and novel physical properties. We show that Mn ions can be controllably doped at either of the perovskite *A* (Sr) or *B* (Ti) site as well as at both sites simultaneously and the resultant physical properties depend intimately on the particular dopant site. We critically review the recent literature on various Mn-doped $SrTiO_3$ systems, which includes reports of dielectric glass, spin-glass and ferromagnetism and by combining experiments with first-principles calculations, we demonstrate that depending on the particular dopant site for Mn ions, the dielectric properties can be widely tuned from a quantum paraelectric to a dielectric glass. However, the intrinsic magnetism in all these cases remains essentially paramagnetic for phase-pure systems.

Keywords. Doping; relaxor; paramagnet.

PACS Nos 75.20.−g; 77.80.Jk; 71.30.+h

1. Introduction

$SrTiO_3$ (STO) is one of the most widely studied materials in condensed matter physics owing to its wide range of functionalities [1], which spans from being a wide-band gap insulator, that is widely used as thin film substrates, to a superconductor [2] when appropriately reduced. Recently, coexistence of two-dimensional electron gas, superconductivity and weak ferromagnetism have been observed at the thin-film heterointerface between the band-insulator $LaAlO_3$ and STO [3,4]. Extensive research has been directed towards achieving multifunctionality by suitable doping of a wide range of transition metal ions and charge carriers into bulk STO [5,6]. While introduction of a dopant ion can destabilize the quantum paraelectric state of STO [7] and likely induce ferroelectricity, a transition-metal dopant ion carries the spin moment which in addition introduces magnetic functionality. In this review, we focus on the dielectric and magnetic properties of bulk Mn-doped STO, which recently has generated tremendous experimental and theoretical research interests. Particularly, by combining experiments with first-principles

calculations, we show that the dielectric properties of STO get significantly altered on doping with Mn, and the site of Mn doping has a marked influence on both the qualitative as well as quantitative dielectric properties. We also discuss the magnetic properties of various Mn-doped systems and our results show that while all phase-pure systems remain essentially paramagnetic without any trace of magnetic ordering down to the lowest temperature, minute spontaneous magnetization signals can emerge by the presence of tiny quantities of magnetic impurity phases in some samples, which often gets overlooked by the routinely employed standard sample characterization techniques.

2. Results and discussion

2.1 *Mn doping in $SrTiO_3$*

STO crystallizes in the cubic space group $Pm\text{-}3m$ which consists of corner-shared TiO_6 octahedra where Ti^{4+} is coordinated by six O^{2-} atoms (as shown in figure 1a) and Sr^{2+} in the cuboctahedral cavity, coordinated by twelve O^{2-} atoms (as shown in figure 1b). As Mn can exist in a wide variety of oxidation states, it can be doped either as Mn^{2+} at the perovskite *A* (Sr) site (SrMn) or as Mn^{4+} at the *B* (Ti) site (TiMn) or simultaneously at both the *A* and *B* sites in the corresponding oxidation states of (2+) and (4+) respectively (SrMnTiMn) [8]. The solubility limit of Mn ions at the *A* site is suggested to be much less (∼3%) compared to that at the *B* site (∼15%) [9], probably driven by the increased thermodynamic stability of the latter configuration [10]. These site-specific Mn dopings in STO can be achieved by the conventional mixed oxide method [8,9], starting with $SrCO_3$, TiO_2 and Mn_2O_3 in stoichiometric amounts. Room-temperature X-ray diffraction (XRD) suggests that all the Mn-doped STO samples (SrMn, TiMn, SrMnTiMn) crystallize in the cubic $Pm\text{-}3m$ space group accompanied by reduced unit-cell sizes due to the smaller ionic radii of Mn ions [8,9].

Electron paramagnetic resonance (EPR) has been widely employed to investigate the valences and local environments of the doped Mn ions in the STO lattice [11–13]. Specifically, characteristic values of hyperfine splittings and Lande *g* factors in the corresponding EPR spectra have been very effective in distinguishing between the SrMn,

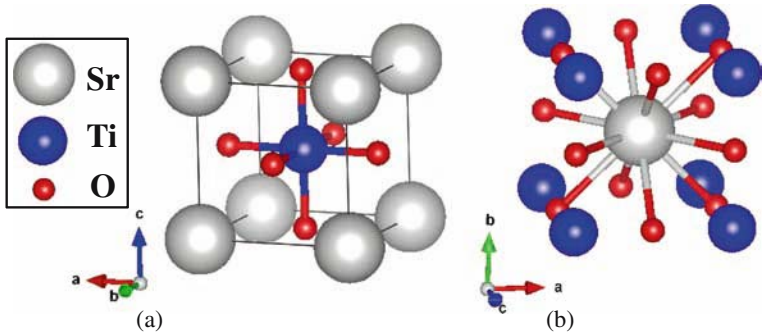

Figure 1. Schematic crystal structure of $SrTiO_3$ showing (**a**) six-oxygen-coordinated Ti and (**b**) twelve-oxygen-coordinated Sr atoms.

TiMn and SrMnTiMn samples [8,14,15]. The room-temperature EPR spectra collected on $Sr_{0.98}Mn_{0.02}TiO_3$ (SrMn), $SrTi_{0.99}Mn_{0.01}O_3$ (TiMn) and $Sr_{0.97}Mn_{0.03}Ti_{0.93}Mn_{0.07}O_3$ (SrMnTiMn) samples are shown in figure 2. The EPR spectrum of SrMn is seen to have a hyperfine splitting of 88 Oe and a Lange g factor of 2.01, which is characteristic of the presence of Mn^{2+} ions doped at the Sr site [13]. The EPR spectra of TiMn sample consist of a sextet of lines with a hyperfine splitting of 74 Oe and a Lande g factor of 1.997, and is characteristic of the expected presence of Mn^{4+} ions doped at the Ti site [11,12]. Further, additional but weak signals (∼5% relative intensity) with hyperfine splittings of 75 Oe (86 Oe) are barely discernible for SrMn (TiMn) in figure 2, suggesting the presence of minute quantities of unintented doping of Mn^{4+} ions at the Ti site (Mn^{2+} doping at the Sr site) for SrMn (TiMn) [15]. Such small complimentary dopings for SrMn and TiMn samples are possibly within the synthetic uncertainties of our mixed-oxide method. Finally, the EPR spectrum of SrMnTiMn sample consists of a broad background, well known to arise at such high Mn concentrations, resulting from dipolar interactions and exchange coupling between the dopant ions [8,15]. However, the same spectrum also consists of finer features riding on the broad background, and these hyperfine-split features show one-to-one correspondences with those of SrMn and TiMn, as shown by the guide lines in figure 2, thus demonstrating that SrMnTiMn consists of two species of doped Mn ions: Mn^{2+} ions doped at the Sr site and Mn^{4+} ions doped at the Ti site as per the synthetic design [8]. Reduced TiMn samples also exhibit EPR signals (sextet pattern with hyperfine splitting of around 84 Oe and Lande g factor of 2.005) due to the presence of Mn^{2+} ions at the octahedral site associated with the presence of oxygen vacancies [14,16,17]. Further, in reduced Mn-doped STO samples, EPR signals corresponding to Mn^{3+}–V_O (V_O denotes an oxygen vacancy site) centres [18] can also be observed. However, the presence of Mn^{3+} ions was ruled out for SrMn or TiMn samples prepared by mixed-oxide methods in air or nitrogen gas atmospheres [15].

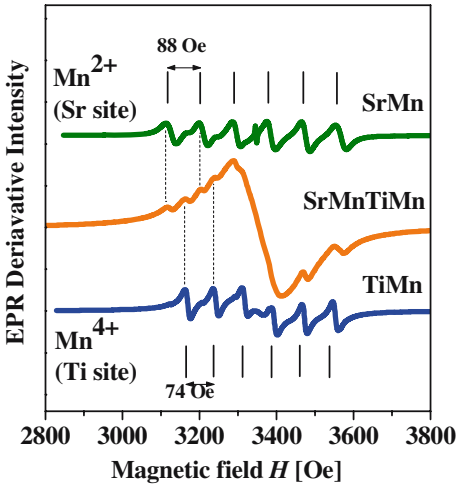

Figure 2. Room-temperature electron paramagnetic resonance (EPR) spectra of SrMn, TiMn and SrMnTiMn (adapted from ref. [8]).

Recent X-ray absorption near-edge structural (XANES) study on TiMn samples suggests ∼7% of Mn^{2+} doping at the Sr site [19], similar to the above EPR results. However, XANES studies on SrMn sample have suggested the presence of significant amounts of Mn^{4+} ions at the Ti site, as large as ∼50% of the total Mn ions [19,20], thus, being in sharp contrast with the corresponding EPR results, which suggest only ∼5% occupancy at the Ti site [15]. We note that these XANES results were mainly based on comparisons with reference compounds containing the same valence state of Mn, namely using $SrMnO_3$ as a reference for TiMn and $MnTiO_3$ for SrMn [19,20]. Surprisingly, the reference compound, i.e. $MnTiO_3$, which was used for SrMn, crystallizes in the ilmenite *R*-3 space group and contains Mn^{2+} ions coordinated with six O^{2-} ions. Thus, the local structure around the Mn^{2+} ions in $MnTiO_3$ is very different from SrMn, which contain Mn^{2+} ions coordinated with twelve O^{2-} ions and in a cubic lattice. $SrMnO_3$, which crystallizes in the hexagonal structure, is in contrast with TiMn which crystallizes in the cubic structure. However, $SrMnO_3$ contains Mn^{4+} ions coordinated with six O^{2-} ions as in TiMn. Thus, although $SrMnO_3$ is partly suitable as a reference compound for TiMn, it is very difficult to get a suitable reference compound for SrMn. In order to further investigate these results, XANES experiments were performed on our SrMn and TiMn samples at the XAFS beamline at Elettra Sincrotrone Centre in Italy. Figures 3a and 3b show the room-temperature Mn *K*-edge XANES spectra of TiMn and SrMn, along with few reference compounds: $SrMnO_3$ [20], $MnTiO_3$ [20] and MnO. As seen by the comparison in figure 3a, the XANES spectra of TiMn can be reasonably well explained using the reference $SrMnO_3$ (as shown by the guidelines, albeit with some differences) suggesting a predominantly *B*-site occupancy as Mn^{4+} ions in TiMn. The XANES spectrum of SrMn, as shown in figure 3b, consists of two spectral regions with strong absorptions, one around 6545 eV and the other around 6554 eV (shown by the dashed lines). $MnTiO_3$ has a large intensity around 6545 eV. However, its absorption drops around 6554 eV, where $SrMnO_3$ has large absorption intensity. This probably prompted Valant *et al* [19] to use a superposition of $MnTiO_3$ and $SrMnO_3$ to act as a reference for SrMn and to assign the respective contributions from $MnTiO_3$ and $SrMnO_3$ to the presences of Mn ions at Sr and Ti sites, respectively. Measurement on MnO, which crystallizes in the cubic Fm-$3m$ space group and consists of Mn^{2+} ions coordinated with six O^{2-} ions, was performed to act as a reference for SrMn. However, as we show in figure 3b, the XANES spectra of the reference compounds for SrMn, namely MnO and $MnTiO_3$, differ both qualitatively and quantitatively between themselves, with MnO having strong absorptions around 6545 and 6554 eV. Thus, although the origin of such features has not been discussed here, the sharp intensity differences between the two reference compounds clearly illustrate the inadequancy of either $MnTiO_3$ or MnO to act as a suitable reference compound for SrMn, and, thus, unlike in refs [19,20], we refrain from performing any quantitative estimates of relative site occupancies from the XANES data.

X-ray absorption spectroscopy (XAS), which is known to provide very distinct Mn $L_{2,3}$ spectral shapes for different valencies of Mn ions [21], was used to distinguish Mn^{2+} dopants at the Sr site from Mn^{4+} dopants at the Ti site [8]. A comparison of the XAS spectral shapes of SrMn and TiMn with the reference compounds, as shown in figures 3c and 3d, clearly establishes the presence of Mn^{2+} valence state in SrMn and Mn^{4+} valence state in TiMn samples. The XAS results, thus, clearly rule out the presence of any significant amount of Mn^{4+} ions in SrMn, as was suggested by the XANES analysis.

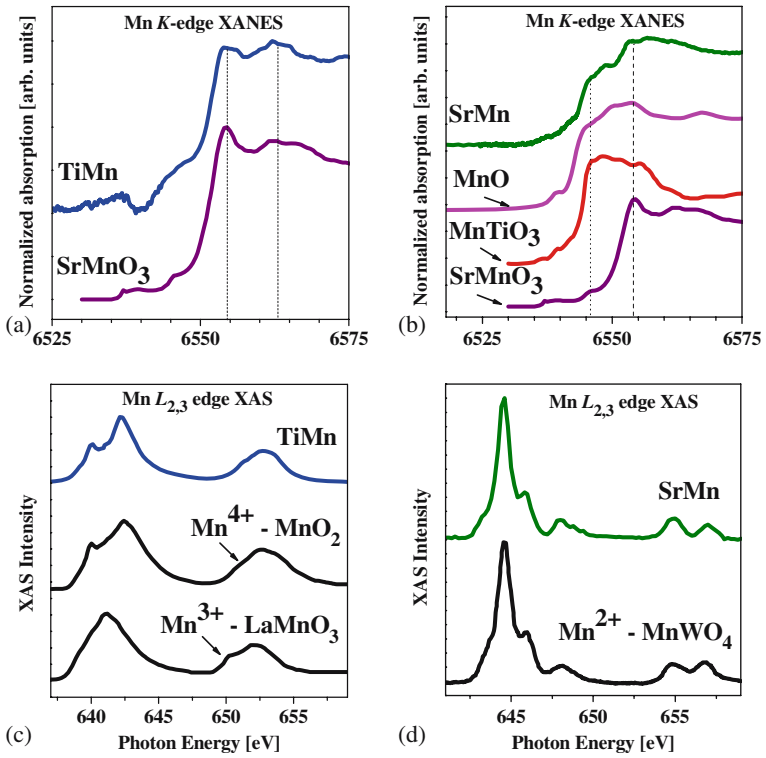

Figure 3. Room-temperature Mn K-edge X-ray absorption near-edge structure (XANES) spectra of (**a**) SrMn, (**b**) TiMn and the Mn $L_{2,3}$-edge X-ray absorption (XAS) spectra of (**c**) SrMn and (**d**) TiMn (panels (**c**) and (**d**) are adapted from ref. [8]).

The presence of small amounts of Mn^{4+} ions in SrMn or Mn^{2+} ions in TiMn, as was suggested by the EPR findings, cannot, however, be ruled out by these XAS data as the signal from such minute contributions may be overwhelmed by the dominant signals from Mn^{2+} and Mn^{4+} in SrMn and TiMn, respectively.

2.2 *Dielectric properties*

Having elaborated on the valences and site occupancies of Mn ions in SrMn, TiMn and SrMnTiMn samples, we shall now discuss their dielectric properties. STO is a quantum paraelectric, which does not undergo any electrical ordering down to ∼0 K. Intriguingly, doping small amounts (∼2%) of Mn ions at the Sr site induces sharp qualitative changes. Figure 4a shows the temperature dependence of the relative dielectric constants (ϵ_r) of SrMn; SrMn exhibits strong dielectric relaxations, with the temperature (T_m) for occurence of the maximum dielectric constant increasing with the increase of the measurement frequency (f_i) [8,22,23]. These dielectric relaxations in SrMn have been understood using a critical slowing down analysis, which is traditionally employed to study the second-order spin glass phase transition [24]; T_m was seen to depend on f_i with

a power-law relation $f_i \sim f_o \times (\frac{T_m}{T_{gl}} - 1)^{z\nu}$ [8,22,23]; T_{gl} (the glass transition temperature) ~ 40 K, $z\nu$ (the critical exponent) ~ 10.6 and f_o (the attempt frequency) $\sim 1.3\times10^6$ Hz was found for SrMn [8]. Such glassy dielectric properties indicate the presence of multiple ground states for the electric polarization in SrMn. As shown by EXAFS [20] and also first-principles calculations [8], Mn ions off-centres from the ideal A-site position in SrMn along the $\langle 0\ 0\ 1\rangle$ direction ($r_A = 1.25$ Å for Mn^{2+} is smaller than $r_A = 1.44$ Å for Sr^{2+}), and as there are six equivalent ways of undergoing this off-centring in a cubic lattice, it gives rise to a large degenerate energy landscape for the orientation of the corresponding electrical dipole moment. In sharp contrast, as seen in figure 4b, TiMn does not exhibit any dielectric relaxations and seemingly retains the quantum paraelectric state as undoped STO [8,25]. Similar quantum paraelectric properties as TiMn have recently been observed in STO doped with other transition metal ions at its B site, like V, Fe, Ni [26]. These results are intriguing because the dielectric properties of STO are intimately related to the Ti $3d^0$ state and, thus, *apriori* B-site doping with a non-$3d^0$ ion is expected to induce drastic qualitative changes. The dielectric properties of SrMn and TiMn also exhibit significant quantitative differences; While ϵ_r of SrMn shows a modest

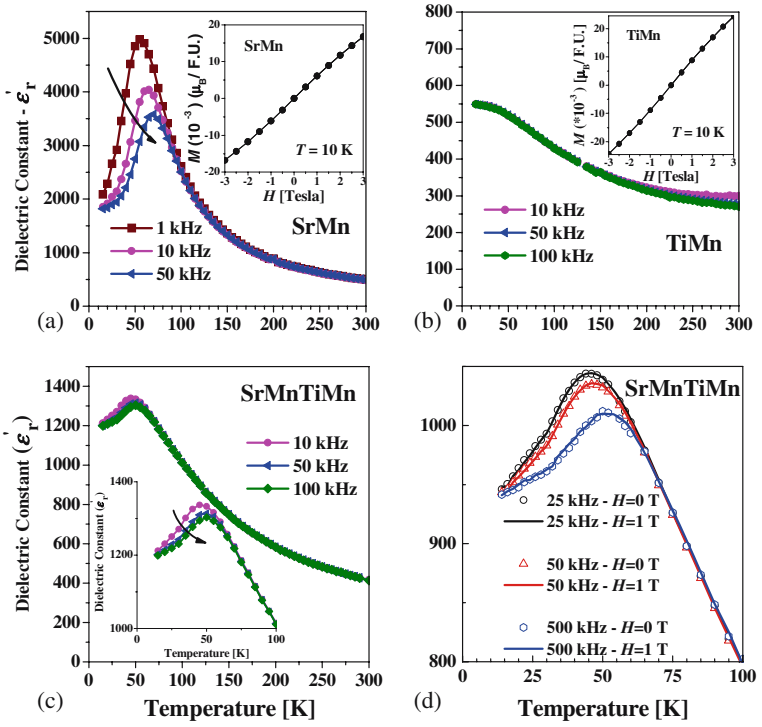

Figure 4. Dielectric constants of (**a**) SrMn, (**b**) TiMn and (**c**) SrMnTiMn. Isothermal magnetization of SrMn (inset of (**a**)) and that of TiMn (inset of (**b**)) showing a linear dependence of magnetization on applied magnetic fields without any hysteresis. (**d**) The dielectric constant of SrMnTiMn in the presence and absence of a magnetic field of 1 Tesla (adapted from ref. [8]).

Table 1. Comparison of dielectric properties of $SrTiO_3$, SrMn, TiMn and SrMnTiMn at 300 K and 1 MHz (adapted from ref. [8]).

	$SrTiO_3$	SrMn	TiMn	SrMnTiMn
ϵ_r'	248	278	140	251
$D = \tan\delta$	0.002	0.005	0.03	0.0003

increase compared to STO, TiMn has a lower dielectric constant. Further, the dielectric loss (D) of SrMn retains a favourable value, whereas D for TiMn is distinctly higher, as shown in table 1. SrMnTiMn also exhibits glassy dielectric properties, with the dielectric constant exhibiting distinct dielectric relaxations, as shown in figure 4c. An analysis of the dielectric relaxations of SrMnTiMn using the same critical slowing down analysis, as employed for SrMn, yields the values of T_{gl}, $z\nu$ and f_o as 35 K, 7.8 and 9×10^7 Hz, respectively [8]. These obtained relaxation constants of SrMnTiMn are very similar to those of SrMn, suggesting that the glassy dielectric properties of SrMnTiMn also arise from off-centric displacements of Mn ions at the Sr site [8]. Quantitatively, SrMnTiMn exhibits distinctly superior dielectric properties, with a lower D (better by an order of magnitude than STO), and still retaining the superior ϵ_r of STO, as shown in table 1.

Comparative analysis of the phonon spectra of STO, TiMn, SrMn and SrMnTiMn provides valuable insights into the origin of such contrasting dielectric properties [8]. Figures 5a and 5b show the total and polar phonon density of states (DoS), respectively at the Gamma point calculated with the corresponding $2\times2\times2$ supercells. The presence of a few unstable modes in the DoS for both undoped and doped STO, as seen in figure 5a, results from the structural optimizations which did not take into consideration the antiferrodistortive rotational motion of the oxygen octahedra [8,27]. However, as these unstable modes are not polar in character, as seen from figures 5a and 5b, they do not affect the calculated dielectric constants. The reduced dielectric constant in TiMn arises from a lowering in the contribution from phonons, mainly arising due to hardening (increase of

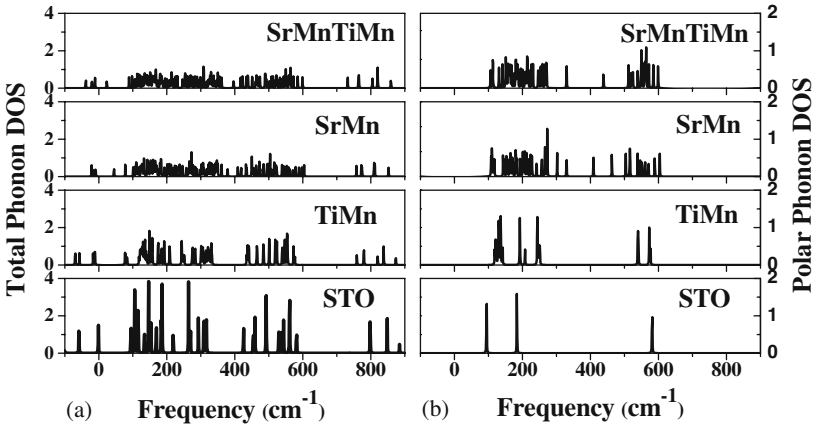

Figure 5. Calculated (**a**) total and (**b**) polar phonon density-of-states at the Γ-point ($q = 0$) for STO, TiMn, SrMn and SrMnTiMn (adapted from ref. [8]).

energy) of phonons driven by the reduction of lattice parameters, and also from increased line broadenings of the IR-active modes due to the broken symmetry in TiMn. Similar effects also occur for SrMn. Further, there is an overall decrease of the Born-effective charges at Ti sites in SrMn as compared to TiMn, thereby leading to increased lowering of the phonon contributions to the dielectric constant in SrMn. Relaxation of the geometry leads to Mn ion off-centring at the Sr site in SrMn [8]. Interestingly, this off-centring gives rise to a large local dipole moment (∼3.9 Debye) in SrMn, which more than compensates for the reduced phononic contributions, thereby accounts for the observed larger dielectric constant values in SrMn, as observed in table 1. The vibration spectra of SrMn, with the presence of significant phonon mode couplings possibly lead to the emergence of the relaxor behaviour in SrMn. In SrMnTiMn, all these factors from both *A* and *B* site dopings contribute to its unique dielectric properties.

2.3 *Magnetic properties*

Magnetism in Mn-doped STO has recently attracted a lot of attention with both claims and counterclaims of the presence of intrinsic spontaneous magnetization in these systems. SrMn has been claimed to be an intrinsic multiglass, where, in addition to the dielectric glassiness, as shown in figure 4a, glassy magnetic properties were also identified around similar temperatures (∼40 K) as the onset of dielectric glassiness [22,23,28]. In sharp contrast to these magnetic results, our earlier detailed magnetic investigations [8] and more recent muon spin relaxation, EPR and magnetization studies [15,19,29] have revealed an essentially paramagnetic state without any kind of magnetic ordering down to the lowest temperature (∼10 K) in phase-pure SrMn samples. In support to the scenario of an extrinsic origin for the observed magnetization in SrMn samples, recent combined magnetization and transmission electron microscopy studies have traced the origin of such extrinsic magnetic signals to the presence of inhomogeneities with clear formation of impurity clusters in improperly processed samples [19].

The magnetization (M) of our SrMn and TiMn, as shown in the insets of figures 4a and 4b, were found to depend linearly on the applied magnetic field (H). TiMn, similar to SrMn, also abstains from any kind of magnetic ordering down to the lowest temperature [8]. Instead, SrMnTiMn sample was seen to exhibit glassy magnetic properties [8], with a clear separation of field-cooled (FC) and zero-field-cooled (ZFC) magnetization data below the ordering temperature (as shown in figure 6a), a clear frequency dependence of the AC susceptibility data and absence of any observable feature in the specific heat around the magnetic ordering temperature [8,30]. Although both SrMn and SrMnTiMn samples exhibited similar dielectric properties, their contrasting magnetic properties clearly suggest decoupling between the dielectric and magnetic glassiness in SrMnTiMn. The decoupling between the dielectric and magnetic glassiness in SrMnTiMn is further evidenced by the absence of any observable magnetocapacitance, as shown in figure 4d [8]. Detailed and extensive structural, Raman and magnetization studies have clearly established the extrinsic origin of the observed glassy magnetization in SrMnTiMn, which was found to originate by the presence of extremely small quantities of Mn_xO_y impurity phases with $x \sim 3$ and $y \sim 4$ (size of the impurity crystallite ∼ 17 nm) [8], which possibly were easily overlooked by standard characterization tools. Figure 6b shows the magnetization signals of various samples of SrMnTiMn which were prepared

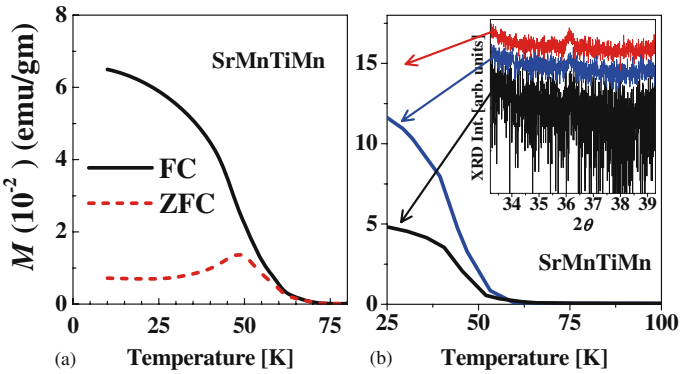

Figure 6. (**a**) Magnetization of SrMnTiMn collected in heating runs after cooling the sample in the presence (FC) or absence (ZFC) of a magnetic field. (**b**) FC magnetization of various samples of SrMnTiMn with their corresponding X-ray diffraction patterns (shown in the inset). A DC magnetic field of 100 Oe was used for these measurements (adapted from ref. [8]).

with the same target composition of $Sr_{0.97}Mn_{0.03}Ti_{0.93}Mn_{0.07}O_3$, and were found to have varying, though extremely minute, quantities of Mn_3O_4 impurity phases (seen as a small peak around $2\theta = 36°$ in the corresponding XRD data when plotted in logarithmic scale as shown in the inset of figure 6b). Interestingly, the magnetization signal of these SrMnTiMn samples were found to be intimately correlated with the corresponding amount of the Mn_3O_4 impurity phases in them, as shown in figure 6b. Mn_3O_4 nanoparticles, exchange-coupled with a naturally grown surface layer of MnO_2, can give rise to spin-glass magnetic properties [31]; Similar mechanism is probably behind the glassy magnetic properties observed in our SrMnTiMn and in the SrMn samples of refs [22] and [23].

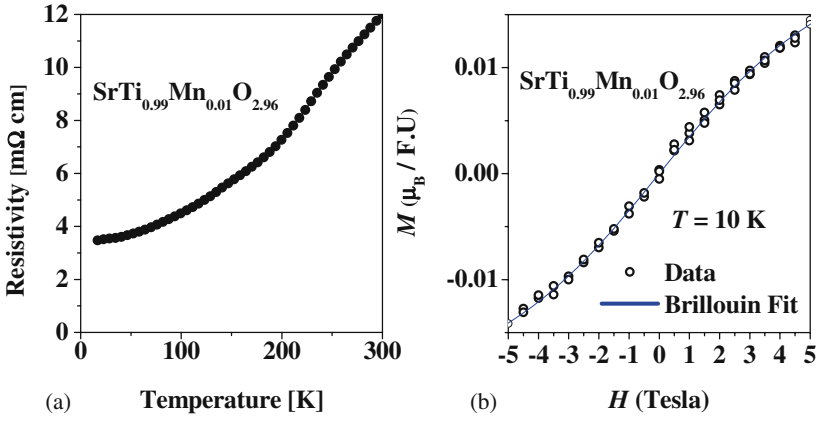

Figure 7. (**a**) Resistance of $SrTi_{0.99}Mn_{0.01}O_{2.96}$ showing its metallicity down to the lowest temperature. (**b**) Isothermal magnetization of $SrTi_{0.99}Mn_{0.01}$ $O_{2.96}$ at $T = 10$ K (symbols) and corresponding paramagnetic Brillouin-function fit (solid line) to the experimental data (adapted from ref. [14]).

In order to attain intrinsic magnetism in Mn-doped STO, charge carriers (electrons) were also doped in STO by the formation of oxygen vacancies [32] resulting in metallic ground states (as shown in figure 7a), as charge carriers are expected to mediate ferromagnetic coupling between localized magnetic moments through one of the several established mechanisms, such as double-exchange [33], RKKY [34–36] and kinetic stability [37]. Intrinsic paramagnetism was, however, observed even in the reduced metallic systems (as illustrated by the excellent agreement between the observed magnetization data and that simulated using paramagnetic Brillouin function in figure 7b) [14]. In sharp contrast, Middey *et al* [16] reported extremely weak ferromagnetism ($\sim$0.04 μ_B per Mn ion) in the reduced Mn-doped STO, which was, however, suggested to have an extrinsic origin in ref. [14], possibly arising from Mn ion clustering.

3. Summary

It has been demonstrated that Mn ions can be controllably doped in STO, with the site of doping being primarily decided from the nominal ionic off-stoichiometries. The site of Mn doping is seen to have a profound influence on the resultant dielectric properties, with the Sr-site-doped STO exhibiting relaxor dielectric properties, whereas the Ti-site-doped compound exhibiting quantum paraelectric properties, similar to the undoped STO. The relaxor dielectric properties of SrMn arises from Mn ion off-centring at the Sr site. The dual-doped compound, where Mn ions substitute both Sr and Ti sites, exhibits relaxor dielectric properties qualitatively similar to Sr-site-doped compound. In addition, it exhibits superior dielectric properties with much reduced dielectric loss ($\sim 10^{-4}$) and large dielectric constant ($\sim$250). Both Sr-site and Ti-site-doped compounds remain paramagnetic down to the lowest measurement temperature. The dual-site doped compound exhibits glassy magnetic properties in addition to glassy dielectric properties. However, the glassy magnetism is seen to have extrinsic origin. Mn-doped STO, when synthesized free of magnetic impurities, is observed to be paramagnetic.

Acknowledgements

DC acknowledges exciting collaboration with S Mukherjee, P Mandal, A Sundaresan, U V Waghmare, S Bhattacharjee, R Mathieu, P Lazor, O Eriksson, B Sanyal, P Nordblad, A Sharma, S V Bhat, B Pal, O Karis, M Unnikrishnan and D D Sarma which contributed to most of the data and ideas presented in this review.

References

[1] J H Haeni, P Irvin, W Chang, R Uecker, P Reiche, Y L Li, S Choudhury, W Tian, M E Hawley, B Craigo, A K Tagantsev, X Q Pan, S K Streiffer, L Q Chen, S W Kirchoefer, J Levy and D G Schlom, *Nature* **430**, 758 (2004)
[2] C S Koonce, M L Cohen, J F Schooley, W R Hosler and E R Pfeiffer, *Phys. Rev.* **163**, 380 (1967)
[3] A Ohtomo and H Y Hwang, *Nature* **427**, 423 (2004)
[4] L Li, C Richter, J Mannhart and R C Ashoori, *Nat. Phys.* **7**, 762 (2011)
[5] J Inaba and T Katsufuji, *Phys. Rev. B* **72**, 052408 (2005)

[6] S X Zhang, S B Ogale, D C Kundaliya, L F Fu, N D Browning, S Dhar, W Ramadan, J S Higgins, R L Greene and T Venkatesan, *Appl. Phys. Lett.* **89**, 012501 (2006)
[7] K A Müller and H Burkard, *Phys. Rev. B* **19**, 3593 (1979)
[8] D Choudhury, S Mukherjee, P Mandal, A Sundaresan, U V Waghmare, S Bhattacharjee, R Mathieu, P Lazor, O Eriksson, B Sanyal, P Nordblad, A Sharma, S V Bhat, O Karis and D D Sarma, *Phys. Rev. B* **84**, 125124 (2011)
[9] A Tkach, P M Vilarinho and A L Kholkin, *Acta Mater.* **53**, 5061 (2005)
[10] J A Dawson, H Chen and I Tanaka, *J. Phys. Chem. C* **118**, 14485 (2014)
[11] A Tkach, P M Vilarinho and A L Kholkin, *Acta Mater.* **54**, 5385 (2006)
[12] K A Müller, *Phys. Rev. Lett.* **2**, 341 (1959)
[13] V V Laguta, I V Kondakova, I P Bykov, M D Glinchuk, A Tkach, P M Vilarinho and L Jastrabik, *Phys. Rev. B* **76**, 054104 (2007)
[14] D Choudhury, B Pal, A Sharma, S V Bhat and D D Sarma, *Sci. Rep.* **3**, 1433 (2013)
[15] A Zorko, P Pregelj, H Luetkens, A-K Axelsson and M Valant, *Phys. Rev. B* **89**, 094418 (2014)
[16] S Middey, C Meneghini and S Ray, *Appl. Phys. Lett.* **101**, 042406 (2012)
[17] R A Serway, W Berlinger, K A Müller and R W Collins, *Phys. Rev. B* **16**, 4761 (1977)
[18] D V Azamat, A Dejneka, J Lancok, V A Trepakov, L Jastrabik and A G Badalyan, *J. Appl. Phys.* **111**, 104119 (2012)
[19] M Valant, T Kolodiazhnyi, I Arcŏn, F Aguesse, A-K Axelsson and N M Alford, *Adv. Func. Mater.* **22**, 2114 (2012)
[20] I Levin, V Krayzman, J C Woicik, A Tkach and P M Vilarinho, *Appl. Phys. Lett.* **96**, 052904 (2010)
[21] K V Shanavas, D Choudhury, I Dasgupta, S M Sharma and D D Sarma, *Phys. Rev. B* **81**, 212406 (2010)
[22] V V Shvartsman, S Bedanta, P Borisov, W Kleeman, A Tkach and P M Vilarinho, *Phys. Rev. Lett.* **101**, 165704 (2008)
[23] W Kleeman, V V Shvartsman, S Bedanta, P Borisov, A Tkach and P M Vilarinho, *J. Phys.: Condens. Matter* **20**, 434216 (2008)
[24] P E Jönsson, *Adv. Chem. Phys.* **128**, 191 (2004)
[25] A Tkach, P M Vilarinho and A Kholkin, *Ferroelectrics* **304**, 87 (2004)
[26] S Maletic, D Maletic, I Petronijevic, J Dojcilovic and D M Popovic, *Chin. Phys. B* **23**, 026102 (2014)
[27] N Sai and D Vanderbilt, *Phys. Rev. B* **62**, 13942 (2000)
[28] A Tkach, P M Vilarinho, W Kleemann, V V Shvartsman, P Borisov and S Bedanta, *Adv. Func. Mater.* **23**, 2229 (2013)
[29] M Valant, T Kolodiazhnyi, I Arčon, F Aguesse, A-K Axelsson and N M Alford, *Adv. Func. Mater.* **23**, 2231 (2013)
[30] The aging and memory features associated with glassy magnetic behaviour of SrMnTiMn was further confirmed using DC magnetization memory experiments, as shown in ref. [8]
[31] F Jiao, A Harrison and P G Bruce, *Angew. Chem. Int. Ed.* **46**, 3946 (2007)
[32] D D Sarma, S R Barman, H Kajueter and G Kotliar, *Europhys. Lett.* **36**, 307 (1996)
[33] P W Anderson and H Hasegawa, *Phys. Rev.* **100**, 675 (1955)
[34] M A Ruderman and C Kittel, *Phys. Rev.* **96**, 99 (1954)
[35] T Kasuya, *Prog. Theor. Phys.* **16**, 45 (1956)
[36] K Yosida, *Phys. Rev.* **106**, 893 (1957)
[37] D D Sarma, P Mahadevan, T Saha-Dasgupta, S Ray and A Kumar, *Phys. Rev. Lett.* **85**, 2549 (2000)